HHS Public Access

Author manuscript

Ann Neurol. Author manuscript; available in PMC 2019 March 13.

Published in final edited form as:

Ann Neurol. 2018 March ; 83(3): 599–611. doi:10.1002/ana.25183.

[18F]AV-1451 tau-PET and primary progressive aphasia

Keith A. Josephs, MD, MST, MSc[1], **Peter R. Martin, MS**[3], **Hugo Botha, MD**[1], **Christopher G. Schwarz, PhD**[6], **Joseph R. Duffy, PhD**[2], **Heather M. Clark, PhD**[2], **Mary M. Machulda, PhD**[4], **Jonathan Graff-Radford, MD**[1], **Stephen D. Weigand, MS**[3], **Matthew L. Senjem, MS**[5,6], **Rene L. Utianski, PhD**[2], **Daniel A. Drubach, MD**[1], **Bradley F. Boeve, MD**[1], **David T. Jones, MD, PhD**[1], **David S. Knopman, MD**[1], **Ronald C. Petersen, MD, PhD**[1], **Clifford R. Jack Jr, MD**[6], **Val J. Lowe, MD**[7], and **Jennifer L. Whitwell, PhD**[6]

[1]Department of Neurology (Behavioral Neurology), Mayo Clinic, Rochester, Minnesota, U.S.A

[2]Department of Neurology (Speech pathology), Mayo Clinic, Rochester, Minnesota, U.S.A

[3]Department of Health Science Research (Biostatistics), Mayo Clinic, Rochester, Minnesota, U.S.A

[4]Department of Psychiatry (Neuropsychology), Mayo Clinic, Rochester, Minnesota, U.S.A

[5]Department of Information Technology, Mayo Clinic, Rochester, Minnesota, U.S.A

[6]Department of Radiology (Neuroradiology), Mayo Clinic, Rochester, Minnesota, U.S.A

[7]Department of Radiology (Nuclear Medicine), Mayo Clinic, Rochester, Minnesota, U.S.A

Abstract

Objectives—To assess [^{18}F]AV-1451 tau-PET uptake patterns across the primary progressive aphasia (PPA) variants (logopenic, semantic and agrammatic), examine regional uptake patterns of [^{18}F]AV-1451 independent of clinical diagnosis, and compare the diagnostic utility of [^{18}F]AV-1451, [^{18}F]-fluorodeoxygluclose (FDG)-PET and MRI to differentiate the PPA variants.

Methods—We performed statistical parametric mapping of [^{18}F]AV-1451 across 40 PPA patients (logopenic-PPA=14, semantic-PPA=13 and agrammatic-PPA=13) compared to 80 cognitively normal, PiB-negative controls, age and gender matched 2:1. Principal component analysis of regional [^{18}F]AV-1451 tau-PET SUVR was performed to understand underlying patterns of [^{18}F]AV-1451 uptake independent of clinical diagnosis. Penalized multinomial regression analyses were utilized to assess diagnostic utility.

Results—Logopenic-PPA showed striking uptake throughout neocortex, particularly temporoparietal, compared to controls, semantic-PPA and agrammatic-PPA. Semantic-PPA and

Corresponding Author: Keith A. Josephs, MD, MST, MSc, Professor of Neurology & Neuroscience, Behavioral Neurology & Movement Disorders, Mayo Clinic, College of Medicine, 200 1st Street S.W., Rochester, MN, 55905, Tele: (507)-538-1038, Fax: (507)-538-6012, josephs.keith@mayo.edu.

Author Contributions

KAJ, PRM, SDW, and JLW contributed to the conception & Design of the Study; KAJ, PRM, HB, CGS, JRD, HMC, MMM, JGR, SDW, MLS, RLU, DAD, BFB, DTJ, DSK, RCP, CRJ, VJL, JLW contributed to the acquisition and analysis of data; KAJ contributed to drafting the manuscript

Potential Conflicts of Interest

Nothing to report

agrammatic-PPA showed milder patterns of focal [^{18}F]AV-1451 uptake. Semantic-PPA showed elevated uptake (left>right) in anteromedial temporal lobes, compared to controls and agrammatic-PPA. Agrammatic-PPA showed elevated uptake (left>right) throughout prefrontal white matter and in subcortical grey matter structures, compared to controls and semantic-PPA. The principal component analysis of regional [^{18}F]AV-1451 indicated two primary dimensions, a severity dimension that distinguished logopenic-PPA from agrammatic-PPA and semantic-PPA, and a frontal-versus-temporal contrast that distinguishes agrammatic-PPA and semantic-PPA cases. Diagnostic utility of [^{18}F]AV-1451was superior to MRI and at least equal to FDG-PET.

Interpretation—[^{18}F]AV-1451binding characteristics differ across the PPA variants, and were excellent at distinguishing between the variants. [^{18}F]AV-1451binding characteristics were as good or better than other brain imaging modalities utilized in clinical practice, suggesting that [^{18}F]AV-1451 may have clinical diagnostic utility in PPA.

Keywords

AV1451; tau-PET; PPA

Primary progressive aphasia (PPA) is an umbrella term that encompasses a group of neurodegenerative syndromes characterized by varying combinations of progressive language impairments[1, 2]. Three clinical variants of PPA have been well described and are well recognized[3]: the agrammatic/non-fluent variant (agPPA) characterized by grammatical errors in speech and writing and sometimes associated with apraxia of speech[4]; the semantic variant (svPPA) characterized by grammatically and prosodically normal (i.e. fluent) speech with poor naming from loss of knowledge about the meaning of words; and the logopenic variant (lvPPA) characterized by hesitant speech from word retrieval problems, poor sentence repetition from impairment of working memory, and phonological errors.

Pathological studies have demonstrated that PPA is associated with a number of different abnormal cellular proteins that do not have perfect associations with the three PPA variants[4–8]. One such protein is the microtubule associated protein, tau, which is the most common abnormal protein found in the brains of patients with PPA[6]. Tau is an important protein that has been linked to the neurodegenerative process in many diseases. Differential splicing of three exons in the tau gene yields three different isoforms of abnormally deposited tau in neurodegenerative diseases[9]: tau with predominantly four microtubule binding domains (4R tau); tau with three microtubule binding domains (3R tau), and tau with almost equal amounts of both (3R+4R tau). Understanding tau isoform deposition is important in PPA because pathological studies have shown an association between lvPPA and 3R+4R tau, and an association between agPPA and 4R tau[4–8]. The svPPA variant is rarely associated with tau isoforms[6, 10], and is more commonly associated with another protein, the TAR DNA binding protein of 43 kDa (TDP-43)[6, 8, 10].

With that said, pathological studies are limited by sampling small pieces of brain tissue and therefore cannot reveal patterns of tau deposition across the whole brain in PPA variants. Recently, tau PET imaging has become available which allows for assessment of tau deposition across the entire brain during life. One imaging ligand, [^{18}F]AV-1451 (formerly 18F-T807), has been shown to specifically bind to tau in humans[11]. More recently, with

autoradiographic studies, it has been shown that [^{18}F]AV-1451 binds robustly to 3R+4R tau, while the binding to 4R tau is inconclusive[12–16]. No neuroimaging studies have investigated tau-PET uptake across all three PPA variants. Hence, binding characteristics across PPA variants remains unknown. It is also unknown whether [^{18}F]AV-1451 could have diagnostic utility in differentiating the three PPA variants, and how it would compare to other brain imaging modalities that are currently utilized for diagnostic purposes.

In this study we aimed to 1) identify the patterns of [^{18}F]AV-1451 uptake across the three PPA variants, 2) describe region-level patterns of [^{18}F]AV-1451 uptake in a parsimonious way, independent of clinical diagnosis, and 3) compare [^{18}F]AV-1451 as a diagnostic tool to other brain imaging modalities that are currently utilized in clinical practice. Our lead hypothesis was that [^{18}F]AV-1451 binding characteristics would differ across the three variants and would allow for the separation of lvPPA (3R+4R tauopathy) from the other two variants. To address our specific aims we performed statistical parametric mapping across the three PPA variants, a principle component analysis based on regional [^{18}F]AV-1451 uptake to identify patterns independent of clinical diagnosis among 40 prospectively recruited PPA subjects and penalized multinomial regression to assess for diagnostic utility.

METHODS

Subjects

Between April 1st, 2016 and December 31st 2017, we recruited 42 patients who presented to Mayo Clinic, Department of Neurology with a progressive language disorder who met International Consensus criteria for PPA[3]. All 42 patients were recruited as part of an NIH-funded grant that aimed to better understand tau-PET uptake with [^{18}F]AV-1451 across the PPA variants (PI, Josephs). All patients consented to having their data utilized for research and the study was approved by the Mayo Clinic Institutional Review Board. Forty-one patients underwent the identical neurological, speech and language, and neuropsychological tests of cognition, and completed a 3.0 tesla volumetric head MRI scan, an [^{18}F]-Fluorodeoxyglucose (FDG)-PET scan, an [^{18}F]AV-1451 tau-PET scan, and a Pittsburgh Compound B (PiB) PET scan to assess for beta-amyloid deposition. One additional patient signed consent but did not complete neuroimaging testing due to claustrophobia and was therefore not included in this study. In addition, one PPA patient could not be sub-classified into one of the three well-recognized PPA variants[3]. As a result, 40 patients were included in this study.

Controls

Using the Mayo Clinic Study of Aging cohort[17] we identified 80 age and gender-matched cognitively unimpaired individuals who did not have evidence of amyloid deposition on PiB-PET to serve as a reference group for regional [^{18}F]AV-1451 levels[18].

Clinical Test Battery

All patients were administered the identical test battery. It included tests of *general cognitive function* (The Montreal Cognitive Assessment)[19], *presence of psychiatric features* (The Neuropsychiatry Inventory- short version)[20], *praxis* (Praxis subtest of the Western Aphasia

Battery)[21], *face recognition* (10-item facial recognition task)[22], *confrontation naming* (The Sydney Language Test for Naming)[23], *single word comprehension* (The Pyramids and Palm Tree Test - Word-Word version)[24], *object knowledge* (The Sydney Language Test for Semantic Association Task)[23], *phonemic fluency* (Letter Fluency Test (FAS))[25], *semantic fluency* (Animal Fluency Test)[25], *behavioral control* (The Cambridge Behavioral Inventory)[26], *visual perceptual abilities* (The Visual Object and Spatial Battery – Fragmented Letters[27], *visual spatial abilities* (The Visual Object and Spatial Battery – Cube analysis)[27] and The Rey–Osterrieth complex figure)[25], *syntactic ability* (The Northwestern Anagram Test)[28], *cognitive speed* (TRAILS Making Test A)[25], *executive function* (TRAILS Making Test B)[25]; *working memory* (Digit Span and Spatial Span)[25], *episodic memory* (The Camden Memory Test – Short Recognition Memory Test for faces)[29], *sentence repetition* (Repetition subtest of the Boston Diagnostic Aphasia Examination)[30] and *motor parkinsonism* (The Movement Disorders Society - Sponsored Revision of the Unified Parkinson's Disease Rating Scale –Part III)[31].

PPA classification

All 40 patients included in this study were evaluated by a behavioral neurologist (KAJ or JGR) and had to first meet root diagnostic criteria for PPA[1, 2] to be included in the study. Each patient was then sub-classified into one of the three PPA variants based on guidelines from the International Consensus Criteria[3]. Diagnoses were made solely on the basis of clinical features, and were made independent of the MRI pattern of atrophy, the FDG-PET pattern of hypometabolism and any results from the [^{18}F]AV-1451 and PiB PET scans. The demographics and clinical features of all 40 PPA patients are shown in Table 1.

Image acquisition

All PET scans were acquired using a PET/CT scanner (GE Healthcare, Milwaukee, Wisconsin) operating in 3D mode. For tau-PET, an intravenous bolus injection of approximately 370MBq (range 333-407 MBq) of [^{18}F]AV-1451 was administered, followed by a 20 minute PET acquisition performed 80 minutes after injection. For FDG-PET, subjects were injected with ^{18}F-FDG of approximately 459 MBq (range 367-576 MBq) and after a 30-minute uptake period an 8-minute 18F-FDG scan was performed. For PiB-PET, subjects were injected with PiB of approximately 628 MBq (range, 385-723 MBq) and after a 40-60 minute uptake period a 20 minute PiB scan was obtained consisting of four 5-minute dynamic frames following a low dose CT transmission scan. Standard corrections were applied. Emission data was reconstructed into a 256×256 matrix with a 30-cm FOV (Pixel size=1.0mm, slice thickness=1.96mm). A global PiB standard uptake value ratio (SUVR) was also generated for each patient in the study, as previously described[32]. All subjects had a 3T MPRAGE sequence performed on the same day as the tau-PET, as previously described[32].

Voxel-level analysis of [^{18}F]AV-1451 in the PPA variants

All image processing steps were performed using SPM12 (www.fil.ion.ucl.ac.uk/SPM). Voxel-level analyses of [^{18}F]AV-1451 were performed to address our first aim. The [^{18}F]AV-1451 images were each registered to the subject's MPRAGE using 6 degrees-of-freedom registration. Normalization parameters were computed between each MPRAGE and

the Mayo Clinic Adult Lifespan Template (MCALT) (https://www.nitrc.org/projects/mcalt/) using ANTs[33]. With these parameters, the MCALT atlases were propagated to native MPRAGE space and all voxels in the [^{18}F]AV-1451 image were divided by the median uptake in the cerebellar crus grey matter to create SUVR images. These SUVR images were normalized to the MCALT and smoothed at 6 mm full-width at half maximum. Voxel-level comparisons were performed comparing each PPA variant to controls using two-sided T-tests in SPM12, with results assessed at $p<0.05$ after cluster-level correction for multiple comparisons using the family wise error correction. Age and gender were included in all first aim analyses as covariates.

Generation of regional data for principal component analyses

To generate region-level data to be used in our second and third aims, the MCALT atlas was transformed into the native space of each MPRAGE, as in the previous section, and used to calculate regional [^{18}F]AV-1451 uptake and FDG-PET metabolism in both the grey and white matter, as well as grey matter volumes. For this study regional values were calculated for the following nine regions-of-interest (ROIs), calculated as voxel weighted medians: *temporal pole* (merged temporal pole mid and temporal pole sup); *lateral temporal cortex* (merged inferior temporal, mid temporal and superior temporal cortices); *entorhinal cortex, fusiform cortex; orbitofrontal cortex* (merged inferior frontal orbital, mid frontal orbital, superior frontal orbital and medial frontal orbital); *medial frontal cortex* (merged superior motor area, anterior cingulum and superior medial frontal); *lateral prefrontal cortex* (merged middle and superior frontal); *Broca's area* (merged inferior frontal operculum and inferior frontal triangularis) and *inferior parietal cortex* (merged inferior parietal, supramarginal and angular). We selected these ROIs as they are typically involved in the different variants of PPA[34, 35]. The entorhinal cortex was selected to represent the medial temporal lobe, instead of the hippocampus, because hippocampal [^{18}F]AV-1451 measurements can be confounded by off-target uptake in the choroid plexus[12, 36]. Median [^{18}F]AV-1451 and FDG-PET values were calculated from both grey and white matter voxels in each ROI and divided by median uptake in cerebellar crus ([^{18}F]AV-1451) or pons (FDG-PET) to create SUVRs. We measured signal only in voxels segmented as tissue in order to compensate for differing amounts of atrophy across subjects, without the noise-boosting and atrophy/tau signal mixing effects commonly associated with partial volume correction. Total intracranial volume (TIV) was also calculated by summing SPM12 grey, white and cerebrospinal fluid segmentations. Log transformed grey matter volumes from each region were then regressed by TIV in 80 healthy age- and sex-matched controls, and standardized residuals were calculated from the model using the log-transformed grey matter volumes for each case. The regional [^{18}F]AV-1451 SUVRs, FDG-PET SUVRs and standardized grey matter volumes were then each entered into separate principal component analyses as described below.

Principal component analyses

To understand and summarize the underlying structure of the ROI-level data, we ran three principal component analyses (PCAs) based on log-transformed [^{18}F]AV-1451 data, log-transformed FDG-PET data, and standardized MRI grey matter volumes from the 40 PPA patients across nine ROIs listed above in each hemisphere. Principal component analysis is an "unsupervised" method in that it is blinded to diagnosis and re-expresses the underlying

structure of a data set as a series of distinct, uncorrelated dimensions. The first principal component (PC-1) is a weighted sum of regional data where the weights are chosen so that PC-1 has maximum variation across subjects. PC-1 can be thought of as the "best" single-number summary of the regional data in a given modality. The second principal component (PC-2) is a weighted sum of regional data with weight chosen so that (a) PC-2 is completely uncorrelated with PC-1 and (b) PC-2 has maximum variation after accounting for PC-1. A data set with k variables can be described in terms of k principal components, each accounting for progressively less variation in the data. Principal component analysis is a tenable tool in regional analyses because of potential drastic reduction the dimensionality of the data without omitting regions while accounting for collinearity of proximally or functionally related regions. All analyses were done using R[37] version 3.4.1.

Voxel-level analysis of [^{18}F]AV-1451 principal components

In order to provide spatial maps describing the loadings of the principal components in the [^{18}F]AV-1451 analysis, voxel-level correlations were performed in SPM12 between the principal component loadings of each patient and [^{18}F]AV-1451 uptake using the template-space smoothed [^{18}F]AV-1451 images created above. These maps were displayed as unthresholded t-statistic maps to show the gradient of positive and negative correlations for loading on each principal component.

Diagnostic Utility of [^{18}F]AV-1451

Penalized multinomial logistic regression was used within each modality to classify cases based on their regional data into the three diagnoses based on their principal component values. Multinomial regression is an extension of binomial logistic regression that allows for more than two outcomes. An optimal ridge penalty determined by leave-one-out cross-validation for each model was used to limit overfitting while retaining all possible predictors (Principal Components) in the model[38]. Models were fit within each modality of scan ([^{18}F]AV-1451 PET, FDG-PET, and MRI) with varying numbers of principal components. Cross-modality comparisons were made using the proportion of cases re-classified correctly in models using the same number of principal components. All analyses were done using R[37] version 3.4.1.

RESULTS

Of the 40 PPA patients in this study, 14 met international criteria for lvPPA, 13 for svPPA and 13 for agPPA. Demographic features were similar across variants although the majority of the lvPPA patients were female (86%), and svPPA patients' median disease duration was 3-years longer than the other two variants at the time of scan. By design, each PPA variant showed the expected pattern of impairment on the battery of administered clinical tests. All lvPPA patients showed beta-amyloid deposition on PiB-PET, and this variant had a higher median PiB SUVR compared to the svPPA and agPPA variants (Table 1).

Voxel-level analysis of [^{18}F]AV-1451 in the PPA variants

Voxel-level maps showing [^{18}F]AV-1451 uptake in the three PPA variants compared to controls are shown in Figure 1. The lvPPA group showed significantly higher uptake

throughout much of the cortex compared to controls, and compared to svPPA and agPPA (Figure 2). Elevated uptake was particularly observed in the left temporoparietal cortex in lvPPA, with additional involvement of the right temporoparietal cortex and frontal lobes. The svPPA and agPPA groups showed much milder patterns of [^{18}F]AV-1451 uptake compared to controls.

The svPPA group showed elevated [^{18}F]AV-1451 uptake bilaterally in the temporal lobes, involving the temporal pole, inferior and middle temporal gyri, fusiform gyrus, amygdala, parahippocampal gyrus and entorhinal cortex, with greater uptake observed in the left hemisphere than the right hemisphere, compared to controls. The svPPA group also showed a region of mild elevated uptake that predominantly included bilateral rectus gyrus, orbitofrontal cortex, nucleus accumbens, anterior striatum and anterior insula compared to controls. The svPPA group showed greater uptake in the temporal pole, amygdala, inferior and middle temporal gyri, fusiform gyrus, parahippocampal gyrus, entorhinal cortex, nucleus accumbens, and anterior insula compared to agPPA (Figure 2). No regions showed greater uptake in svPPA compared to lvPPA.

The agPPA group showed moderately elevated [^{18}F]AV-1451 uptake throughout the white matter of the prefrontal lobe, including orbitofrontal, inferior, middle and superior regions, and temporal lobe, with greater uptake in the left hemisphere, compared to controls. Elevated uptake was also observed in subcortical grey matter structures, including bilateral thalamus, putamen and globus pallidus, with greater uptake observed in the left hemisphere compared to the right hemisphere. The agPPA group showed greater uptake in the left prefrontal white matter, superior putamen and thalamus compared to svPPA (Figure 2). No regions showed greater uptake in agPPA compared to lvPPA.

Representative [^{18}F]AV-1451 images for each of the three PPA variants are shown in Figure 3.

Principal component analysis of [^{18}F]AV-1451, FDG-PET and MRI

Figure 4 shows the actual [^{18}F]AV-1451 SUVRs for all PPA patients. All 14 lvPPA patients had higher mean SUVRs than any of the agPPA and svPPA patients, who tended to be intermixed. The [^{18}F]AV-1451 principal components analysis suggested an underlying two-dimensional structure in the regional data as the first component accounted for 81% (SD 3.83) of the variation and the second component accounted for an additional 7% (SD 1.15). Table 2 shows the loadings of these two principal components for the ROIs and Figure 5 shows voxel-level correlations between [^{18}F]AV-1451 uptake and the loadings of the two principal components. We interpret the first principal component (PC-1) as an overall tau severity measure since the ROI loadings are all of the same sign and essentially the same magnitude. The voxel-level maps similarly illustrate a negative correlation between the loading on PC-1 and [^{18}F]AV-1451 in much of the cortex, particularly in temporoparietal and frontal regions (Figure 5), implying that a greater negative loading is associated with greater [^{18}F]AV-1451 binding in these areas. We interpret the second principal component (PC-2) as a dimension representing a contrast between frontal and temporal regions. That is, after accounting for severity summarized in PC-1, PC-2 locates individuals on a spectrum ranging from relatively high temporal uptake and relatively low frontal uptake to relatively

low temporal uptake and relatively high frontal uptake. This is illustrated in Figure 5 where a negative correlation is observed between PC-2 loading and medial and lateral temporal lobe [^{18}F]AV-1451 uptake, and a positive correlation between loadings and uptake in the prefrontal cortex.

The plot in Figure 6 shows the separation of the three PPA variants according to PC-1 and PC-2 that were calculated from the principal component analysis using the ROI data from each of the three modalities. For [^{18}F]AV-1451, all lvPPA patients were more severe than average (i.e., to the left of the mean on the PC-1 axis in Figure 6) with this dimension discriminating perfectly between lvPPA and the other two variants (area under the receiver operator curve=1, $p<0.001$). After accounting for severity, if we look at the PC-2 axis, we see perfect separation of the agPPA and svPPA patients (area under the receiver operator curve=1, $p<0.001$). In other words, a combination of higher uptake in frontal regions and relatively reduced uptake in temporal regions effectively distinguish agPPA and svPPA.

The penalized multinomial logistic regression models show that [^{18}F]AV-1451 outperformed both FDG-PET and MRI when using two principal components (Figure 6). When considering from three to seven principal components, [^{18}F]AV-1451 and FDG-PET were comparable while both consistently outperformed MRI (Figure 6). These penalized models provide a fair estimate of the ability of these different scan modalities to discriminate between these three diagnoses, showing stronger signals in [^{18}F]AV-1451 and FDG-PET than MRI.

INTERPRETATION

[^{18}F]AV-1451 patterns of uptake were different across the three PPA variants, as we had hypothesized. The patterns differed in terms of severity of binding, regions of uptake, and relative involvement of grey vs white matter. Taking all these differences into account, we show that [^{18}F]AV-1451 patterns of uptake can be utilized to predict clinical diagnosis of the PPA variants at a single subject level with a relatively high degree of accuracy. We found [^{18}F]AV-1451 PET to be as good as FDG-PET and better than MRI at predicting clinical diagnosis.

One of the most striking observations of the study was the significant amount of [^{18}F]AV-1451 uptake in the lvPPA variant compared to controls and compared to svPPA and agPPA. Three other small case series have also observed uptake of [^{18}F]AV-1451 in lvPPA[39–41]. Given that autoradiographic studies show [^{18}F]AV-1451 binds strongly to 3R +4R tau, and the fact that pathological studies have found lvPPA is associated with 3R+4R tau, it is reasonable to deduce that [^{18}F]AV-1451 uptake in lvPPA would highly correlate with tau burden in the brain at the time of scan. Further supporting this notion is the fact that the asymmetric uptake, most severely involving the left temporoparietal cortex, that we observed with [^{18}F]AV-1451 uptake in lvPPA is similar to what has been observed in pathological studies of tau neurofibrillary tangle deposition in lvPPA[8, 42]. The regions of increased uptake identified in our lvPPA patients were similar to the regions reported in the three other [^{18}F]AV-1451 studies and are the same regions that are structurally and functionally most involved in lvPPA[39–41]. The degree of [^{18}F]AV-1451 uptake observed in

lvPPA is not likely to reflect clinical severity given that performance on a test of general cognitive performance, as well as disease duration, was similar in lvPPA compared to the other two groups.

Unlike with lvPPA, [^{18}F]AV-1451 uptake in svPPA was more focal, predominantly involving regions of the temporal lobe, as well as ventromedial frontal regions, that are often atrophic and functionally impaired in svPPA[43]. Given that pathological studies have identified TDP-43, and not tau, as being most strongly associated with svPPA[6, 8, 10], and autoradiographic studies of svPPA with TDP-43 have found little evidence for [^{18}F]AV-1451 binding[12–14], it is unclear what elevated [^{18}F]AV-1451 uptake represents in svPPA. The regions that showed uptake in our studies were also reported to be involved in two other studies of [^{18}F]AV-1451 uptake in svPPA[44, 45], and one study with a different ligand, THK-5351[46]. Therefore, it is worthwhile to consider carefully what [^{18}F]AV-1451 may be binding to in svPPA. Further arguing against [^{18}F]AV-1451 binding to TDP-43 is the fact that TDP-43 deposition in svPPA also occurs to a similar density in regions outside of those that showed [^{18}F]AV-1451 uptake, such as the middle frontal and inferior parietal cortex[10]. Although not very likely, we cannot exclude the possibility that there is some focal 3R + 4R tau that is being detected by [^{18}F]AV-1451in svPPA. We also have to consider the possibility of some off-target binding to something that is focally present in the regions of most severe neurodegeneration such as heme by-products, iron, calcium, or something else. Regardless, off-target binding is a very plausible explanation for the uptake in svPPA as elevated uptake of [^{18}F]AV-1451 has been observed in meningioma's, vascular malformations, and infarctions, for example[47, 48], where there is no good evidence that 3R+4R tau is present.

Similar to svPPA, [^{18}F]AV-1451 uptake in agPPA was less robust and more focal compared to lvPPA. Uptake was observed in frontal and basal ganglia regions that are typically atrophic and functionally impaired in agPPA. What was most noticeable regarding [^{18}F]AV-1451 uptake in agPPA was that uptake in the frontal lobes was limited to white matter. This suggests that whatever [^{18}F]AV-1451 is binding to in agPPA is present in the subcortical white matter but not the cortical grey matter. We also observed greater [^{18}F]AV-1451 uptake in subcortical grey matter structures in agPPA compared to controls and svPPA. More specifically, we noted elevated uptake in the thalamus, globus pallidus and putamen. Off-target binding of the ligand has been observed in these subcortical structures in healthy controls[12] and typically increases with age[49]. However, since we compared our patients to age-matched healthy, PiB-negative, controls it is possible that this finding is disease specific. Involvement of the thalamus, globus pallidus and putamen is reminiscent of the pattern of [^{18}F]AV-1451 uptake that has been observed in another neurodegenerative syndrome, Richardson's syndrome[49, 50]. Intriguingly, both agPPA and Richardson's syndrome are strongly associated with a 4R tauopathy known as progressive supranuclear palsy. It is unclear, however, whether [^{18}F]AV-1451 binds to 4R tau[12–15]. We suspect that whatever target [^{18}F]AV-1451 is binding to in agPPA may be the same target it is binding to in 4R tauopathies such as progressive supranuclear palsy. It is less clear whether the binding targets are similar between agPPA and svPPA (a non 4R tauopathy).

The elevated uptake of [^{18}F]AV-1451 in the three PPA variants is worthy of further discussion. Uptake in svPPA and agPPA challenges the notion that [^{18}F]AV-1451 binding is

100% specific to tau, and argues that the ligand has incomplete specificity. Therefore, although binding in lvPPA is likely to highly correlate with underlying 3R+ 4R tau, there is a high chance that even in lvPPA uptake reflects the sum of specific and non-specific binding; a similar situation may be occurring in agPPA and svPPA. With that said, the findings from this study are still valuable and significant because [^{18}F]AV-1451 uptake did provide excellent discrimination of the three PPA variants.

Our analyses to examine the underlying structure of the regional data showed that [^{18}F]AV-1451 uptake was clearly distinct in terms of severity with lvPPA showing elevated uptake compared to svPPA and agPPA. This suggests that given a diagnosis of PPA, predicting lvPPA based on [^{18}F]AV-1451 requires only taking into account the degree of uptake across these nine ROIs. It was unnecessary to consider the specific pattern of uptake in order to predict lvPPA, although we could hypothesize that accounting for pattern could provide even greater predictive value for lvPPA cases, especially those cases that show relatively lower degrees of [^{18}F]AV-1451 uptake. The degree of tau uptake did not, however, allow prediction of svPPA over agPPA; this is where the contrasting pattern of frontal versus temporal [^{18}F]AV-1451 uptake was useful. Based on results from this study, it appears that a pattern of [^{18}F]AV-1451 uptake that involves frontal regions more than temporal regions suggests a diagnosis of agPPA over svPPA, while a pattern of [^{18}F]AV-1451 uptake that involves the anteromedial temporal lobe regions more than the frontal regions suggests a diagnosis of svPPA. Therefore, although [^{18}F]AV-1451 may prove not to be a stand-alone diagnostic tool to predict the underlying pathologies of the PPA variants, the degree and patterns of uptake may still be helpful to differentiate the variants.

We compared the diagnostic utility of [^{18}F]AV-1451 to FDG-PET and MRI volumes, given that both modalities are commonly utilized in clinical practice to distinguish between PPA variants. [^{18}F]AV-1451 was found to be as good as FDG-PET, and better than MRI, to discriminate between PPA variants. In fact, one could argue that [^{18}F]AV-1451 is the best of the three imaging modalities, given that with just two principal components it had the best discriminatory value, and the fact that the loadings showed that a simple diagnostic algorithm first accounting for uptake severity followed by frontal vs temporal uptake was all that was needed for almost perfect prediction; similar predictive power with FDG-PET required at least three principal components. Regardless, these findings further support the notion that [^{18}F]AV-1451 may be a useful added diagnostic tool in PPA and could provide added diagnostic value with multimodality imaging, i.e.,[^{18}F]AV-1451, FDG-PET and MRI.

The strengths of this study are that all patients were well characterized clinically and that all 120 patients and healthy controls underwent identical imaging protocols. Holding acquisition and analysis parameters constant allows for a more confident comparison of results. In addition, our principal component analysis was unsupervised, allowing us to assess variability in uptake, metabolism and volumes unbiased by clinical diagnosis. The lack of autopsy confirmation is a limitation and it is possible that some of our agPPA and svPPA patients may share the same underlying pathology, such as Pick's disease in which [^{18}F]AV-1451 binding characteristics are unknown, and autoradiographic findings are unclear[12]. Other limitations of this study include the relatively small sample size and the possibility of participation or other selection biases.

The findings from this study reveal that [^{18}F]AV-1451 has potential to differentiate the PPA variants and to be utilized as a diagnostic tool. However, the lack of a credible biological explanation for the elevated uptake in svPPA and agPPA make it less appealing as a biomarker, at present. What is critically needed is to understand what the ligand is binding to in cases that lack pathological evidence for the presence of 3R+4R tau.

Acknowledgments

This study was funded by NIH-grants R21- NS94684, R01-AG50603, R01-DC12519 and U01 AG006786, Mayo Clinic Radiology Research and support from the Elsie and Marvin Dekelboum Family Foundation. We would like to acknowledge AVID Radiopharmaceuticals for provision of AV-1451 precursor, chemistry production advice and oversight, and FDA regulatory cross-filing permission and documentation needed for this work.

References

1. Mesulam MM. Slowly progressive aphasia without generalized dementia. Ann Neurol. 1982 Jun; 11(6):592–8. [PubMed: 7114808]
2. Mesulam MM. Primary progressive aphasia. Ann Neurol. 2001 Apr; 49(4):425–32. [PubMed: 11310619]
3. Gorno-Tempini ML, Hillis AE, Weintraub S, et al. Classification of primary progressive aphasia and its variants. Neurology. 2011 Mar 15; 76(11):1006–14. [PubMed: 21325651]
4. Josephs KA, Duffy JR, Strand EA, et al. Clinicopathological and imaging correlates of progressive aphasia and apraxia of speech. Brain. 2006 Jun; 129(Pt 6):1385–98. [PubMed: 16613895]
5. Deramecourt V, Lebert F, Debachy B, et al. Prediction of pathology in primary progressive language and speech disorders. Neurology. 2010 Jan 5; 74(1):42–9. [PubMed: 19940270]
6. Josephs KA, Hodges JR, Snowden JS, et al. Neuropathological background of phenotypical variability in frontotemporal dementia. Acta Neuropathol. 2011 Aug; 122(2):137–53. [PubMed: 21614463]
7. Spinelli EG, Mandelli ML, Miller ZA, et al. Typical and atypical pathology in primary progressive aphasia variants. Ann Neurol. 2017 Mar; 81(3):430–43. [PubMed: 28133816]
8. Mesulam MM, Weintraub S, Rogalski EJ, Wieneke C, Geula C, Bigio EH. Asymmetry and heterogeneity of Alzheimer's and frontotemporal pathology in primary progressive aphasia. Brain. 2014 Apr; 137(Pt 4):1176–92. [PubMed: 24574501]
9. Goedert M, Spillantini MG, Jakes R, Rutherford D, Crowther RA. Multiple isoforms of human microtubule-associated protein tau: sequences and localization in neurofibrillary tangles of Alzheimer's disease. Neuron. 1989 Oct; 3(4):519–26. [PubMed: 2484340]
10. Josephs KA, Stroh A, Dugger B, Dickson DW. Evaluation of subcortical pathology and clinical correlations in FTLD-U subtypes. Acta Neuropathol. 2009 Sep; 118(3):349–58. [PubMed: 19455346]
11. Xia CF, Arteaga J, Chen G, et al. [(18)F]T807, a novel tau positron emission tomography imaging agent for Alzheimer's disease. Alzheimers Dement. 2013 Nov; 9(6):666–76. [PubMed: 23411393]
12. Lowe VJ, Curran G, Fang P, et al. An autoradiographic evaluation of AV-1451 Tau PET in dementia. Acta Neuropathol Commun. 2016 Jun 13.4(1):58. [PubMed: 27296779]
13. Marquie M, Normandin MD, Vanderburg CR, et al. Validating novel tau positron emission tomography tracer [F-18]-AV-1451 (T807) on postmortem brain tissue. Ann Neurol. 2015 Nov; 78(5):787–800. [PubMed: 26344059]
14. Sander K, Lashley T, Gami P, et al. Characterization of tau positron emission tomography tracer [18F]AV-1451 binding to postmortem tissue in Alzheimer's disease, primary tauopathies, and other dementias. Alzheimers Dement. 2016 Nov; 12(11):1116–24. [PubMed: 26892233]
15. Marquie M, Normandin MD, Meltzer AC, et al. Pathological correlations of [F-18]-AV-1451 imaging in non-alzheimer tauopathies. Ann Neurol. 2017 Jan; 81(1):117–28. [PubMed: 27997036]

16. Josephs KA, Whitwell JL, Tacik P, et al. [18F]AV-1451 tau-PET uptake does correlate with quantitatively measured 4R-tau burden in autopsy-confirmed corticobasal degeneration. Acta Neuropathol. 2016 Dec; 132(6):931–3. [PubMed: 27645292]
17. Roberts RO, Geda YE, Knopman DS, et al. The Mayo Clinic Study of Aging: design and sampling, participation, baseline measures and sample characteristics. Neuroepidemiology. 2008; 30(1):58–69. [PubMed: 18259084]
18. Lowe V, Wiste H, Senjem M, et al. Widespread Brain Tau on Molecular Imaging and its Association with Aging, Braak Stage, and Alzheimer's Dementia Brain. 2017 In Press.
19. Nasreddine ZS, Phillips NA, Bedirian V, et al. The Montreal Cognitive Assessment, MoCA: a brief screening tool for mild cognitive impairment. J Am Geriatr Soc. 2005 Apr; 53(4):695–9. [PubMed: 15817019]
20. Kaufer DI, Cummings JL, Ketchel P, et al. Validation of the NPI-Q, a brief clinical form of the Neuropsychiatric Inventory. J Neuropsychiatry Clin Neurosci. 2000 Spring;12(2):233–9. [PubMed: 11001602]
21. Kertesz, A. Western Aphasia Battery. San Antonio, Tx: PsychCorp; 2007. (Revised)
22. Josephs KA, Duffy JR, Strand EA, et al. Characterizing a neurodegenerative syndrome: primary progressive apraxia of speech. Brain. 2012 May; 135(Pt 5):1522–36. [PubMed: 22382356]
23. Savage S, Hsieh S, Leslie F, Foxe D, Piguet O, Hodges JR. Distinguishing subtypes in primary progressive aphasia: application of the Sydney language battery. Dement Geriatr Cogn Disord. 2013; 35(3–4):208–18. [PubMed: 23467307]
24. Howard, D., Patterson, K. Pyramids and Palm Trees: A test of semantic access from pictures and words Bury St Edmunds. Thames Valley Publishing Company; 1992.
25. Lezak, MD., Howieson, DB., Bigler, ED., Tranel, D. Neuropsychological Assessment. 5th. New York: Oxford University Press; 2012.
26. Bozeat S, Gregory CA, Ralph MA, Hodges JR. Which neuropsychiatric and behavioural features distinguish frontal and temporal variants of frontotemporal dementia from Alzheimer's disease? J Neurol Neurosurg Psychiatry. 2000 Aug; 69(2):178–86. [PubMed: 10896690]
27. Warrington, EK., James, M. The visual object and space perception battery. Bury St Edmonds, UK: Thames Valley Test Company; 1991.
28. Weintraub S, Mesulam MM, Wieneke C, Rademaker A, Rogalski EJ, Thompson CK. The northwestern anagram test: measuring sentence production in primary progressive aphasia. Am J Alzheimers Dis Other Demen. 2009 Oct-Nov;24(5):408–16. [PubMed: 19700669]
29. Clegg F, Warrington EK. Four easy memory tests for older adults. Memory. 1994 Jun; 2(2):167–82. [PubMed: 7584290]
30. Goodglass, H., Kaplan, E., Barresi, B. The Boston Diagnostic Aphasia Examination (BDAE). Baltimore: Lippincott, Williams and Wilkins; 2001.
31. Goetz CG, Tilley BC, Shaftman SR, et al. Movement Disorder Society-sponsored revision of the Unified Parkinson's Disease Rating Scale (MDS-UPDRS): scale presentation and clinimetric testing results. Mov Disord. 2008 Nov 15; 23(15):2129–70. [PubMed: 19025984]
32. Jack CR Jr, Lowe VJ, Senjem ML, et al. 11C PiB and structural MRI provide complementary information in imaging of Alzheimer's disease and amnestic mild cognitive impairment. Brain. 2008 Mar; 131(Pt 3):665–80. [PubMed: 18263627]
33. Avants BB, Epstein CL, Grossman M, Gee JC. Symmetric diffeomorphic image registration with cross-correlation: evaluating automated labeling of elderly and neurodegenerative brain. Med Image Anal. 2008 Feb; 12(1):26–41. [PubMed: 17659998]
34. Botha H, Duffy JR, Whitwell JL, et al. Classification and clinicoradiologic features of primary progressive aphasia (PPA) and apraxia of speech. Cortex. 2015 Aug.69:220–36. [PubMed: 26103600]
35. Rabinovici GD, Jagust WJ, Furst AJ, et al. Abeta amyloid and glucose metabolism in three variants of primary progressive aphasia. Ann Neurol. 2008 Oct; 64(4):388–401. [PubMed: 18991338]
36. Ikonomovic MD, Abrahamson EE, Price JC, Mathis CA, Klunk WE. [F-18]AV-1451 positron emission tomography retention in choroid plexus More than "off-target" binding. Ann Neurol. 2016 Aug; 80(2):307–8. [PubMed: 27314820]

37. R Core team. R: A language and environment for statistcial computing. Austria, Vienna: R Foundation for Statistical Computing; 2017.
38. Hastie, T., Tibshirani, R., Friedman, JH. The Elements of Statistical Learning: Data Mining, Inference, and Prediction: with 200 Full-Color Illustrations. New York: Springer; 2001.
39. Nasrallah IM, Chen YJ, Hsieh MK, et al. 18F-Flortaucipir PET-MRI correlations in non-amnestic and amnestic variants of Alzheimer Disease. J Nucl Med. 2017 Jul.:26.
40. Ossenkoppele R, Schonhaut DR, Scholl M, et al. Tau PET patterns mirror clinical and neuroanatomical variability in Alzheimer's disease. Brain. 2016 May; 139(Pt 5):1551–67. [PubMed: 26962052]
41. Xia C, Makaretz SJ, Caso C, et al. Association of In Vivo [18F]AV-1451 Tau PET Imaging Results With Cortical Atrophy and Symptoms in Typical and Atypical Alzheimer Disease. JAMA Neurol. 2017 Apr 01; 74(4):427–36. [PubMed: 28241163]
42. Josephs KA, Dickson DW, Murray ME, et al. Quantitative neurofibrillary tangle density and brain volumetric MRI analyses in Alzheimer's disease presenting as logopenic progressive aphasia. Brain Lang. 2013 Nov; 127(2):127–34. [PubMed: 23541297]
43. Mummery CJ, Patterson K, Price CJ, Ashburner J, Frackowiak RS, Hodges JR. A voxel-based morphometry study of semantic dementia: relationship between temporal lobe atrophy and semantic memory. Ann Neurol. 2000 Jan; 47(1):36–45. [PubMed: 10632099]
44. Bevan-Jones WR, Cope TE, Jones PS, et al. [18F]AV-1451 binding in vivo mirrors the expected distribution of TDP-43 pathology in the semantic variant of primary progressive aphasia. J Neurol Neurosurg Psychiatry. 2017 Sep 14.
45. Makaretz SJ, Quimby M, Collins J, et al. Flortaucipir tau PET imaging in semantic variant primary progressive aphasia. J Neurol Neurosurg Psychiatry. 2017 Oct 06.
46. Lee H, Seo S, Lee SY, et al. [18F]-THK5351 PET Imaging in Patients With Semantic Variant Primary Progressive Aphasia. Alzheimer Dis Assoc Disord. 2017 Oct 12.
47. Lockhart SN, Ayakta N, Winer JR, La Joie R, Rabinovici GD, Jagust WJ. Elevated 18F-AV-1451 PET tracer uptake detected in incidental imaging findings. Neurology. 2017 Mar 14; 88(11):1095–7. [PubMed: 28188303]
48. Bruinsma TJ, Johnson DR, Fang P, et al. Uptake of AV-1451 in meningiomas. Ann Nucl Med. 2017 Sep 08.
49. Cho H, Choi JY, Hwang MS, et al. Subcortical 18 F-AV-1451 binding patterns in progressive supranuclear palsy. Mov Disord. 2017 Jan; 32(1):134–40. [PubMed: 27813160]
50. Whitwell JL, Lowe VJ, Tosakulwong N, et al. [18 F]AV-1451 tau positron emission tomography in progressive supranuclear palsy. Mov Disord. 2017 Jan; 32(1):124–33. [PubMed: 27787958]

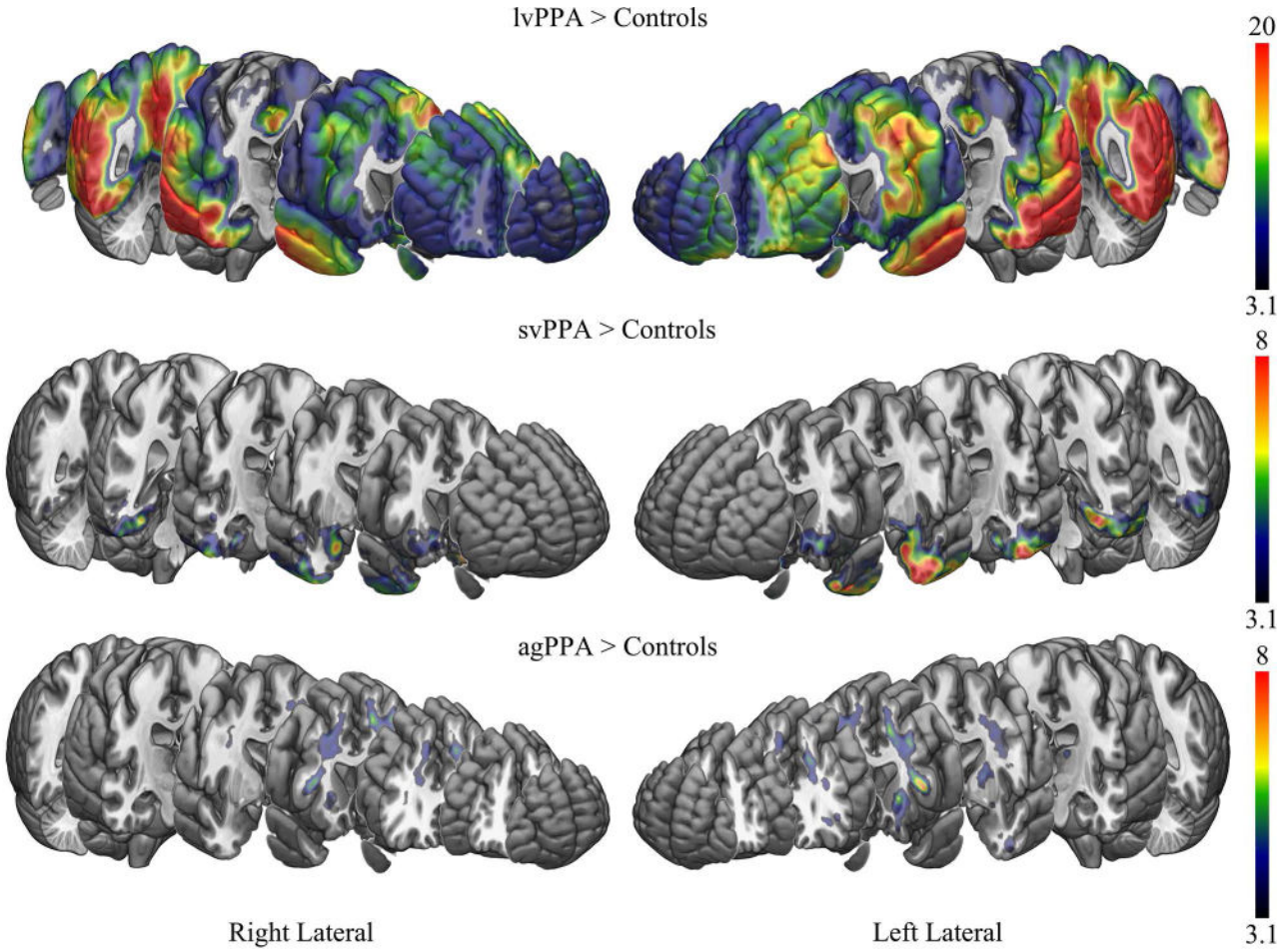

Figure 1.

[^{18}F]AV-1451 patterns of uptake in the three PPA variants compared to controls. Results are shown after cluster-level correction for multiple comparisons using the family wise error correction at $p<0.05$. Results are shown on the MNI152 template using MRICroGL. Scales represent T-score.

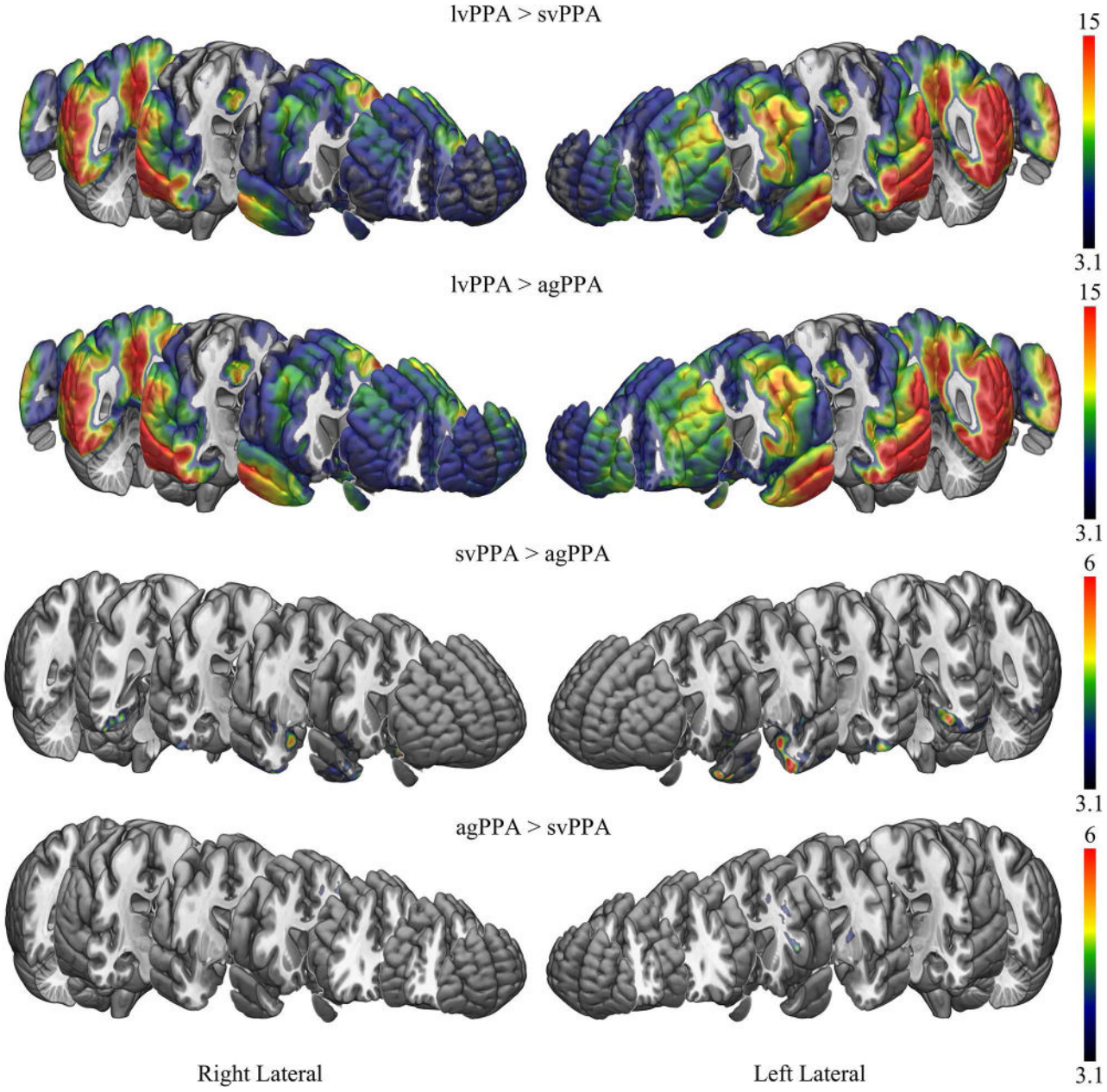

Figure 2.

[^{18}F]AV-1451 patterns of uptake comparing the PPA variants to each other. Results are shown after cluster-level correction for multiple comparisons using the family wise error correction at $p<0.05$. Results are shown on the MNI152 template using MRICroGL. Scales represent T-score.

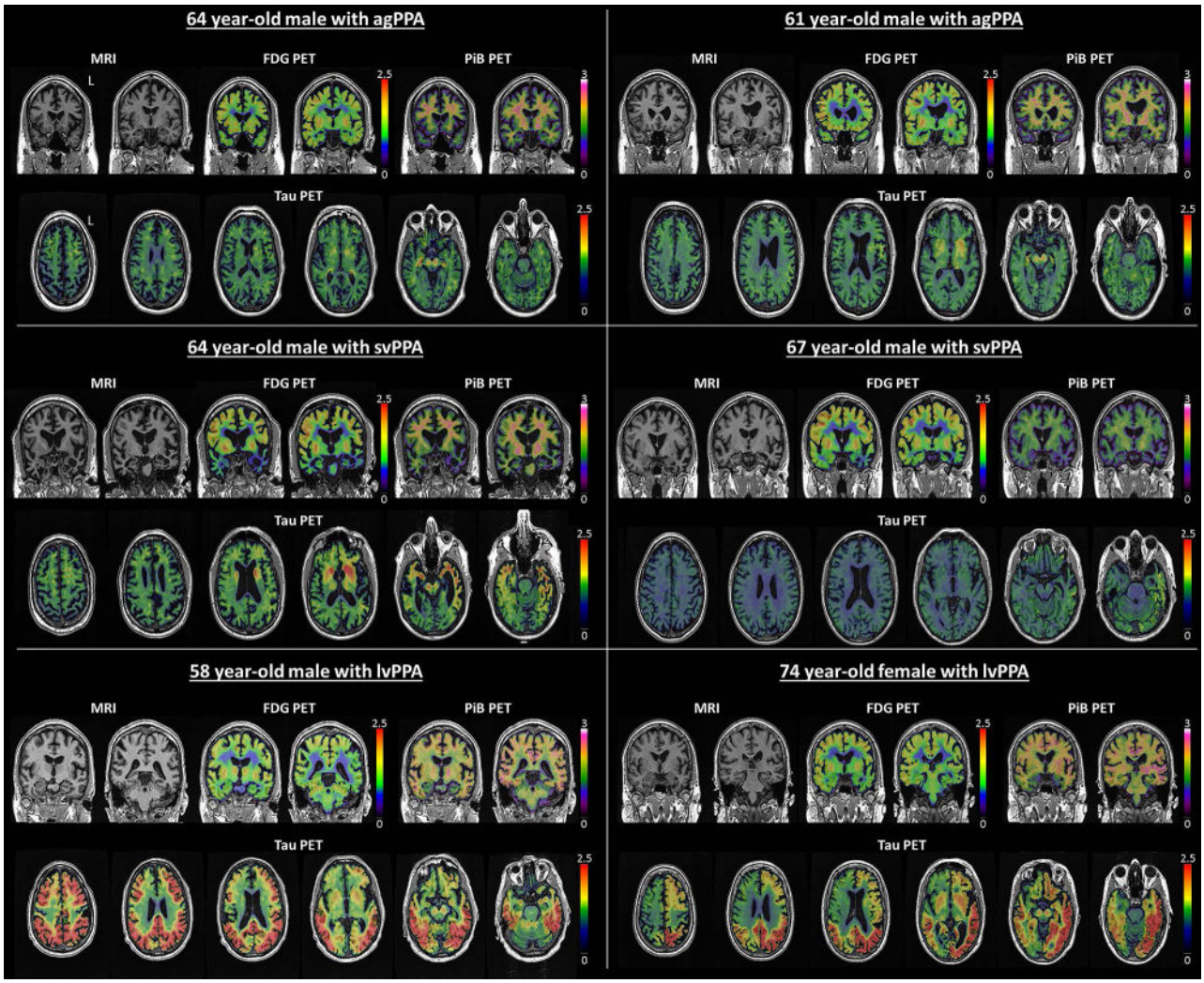

Figure 3.

Individual [^{18}F]AV-1451 tau-PET, FDG-PET, PiB-PET and MRI images from two agPPA, two svPPA and two lvPPA subjects. Scales represent SUVR.

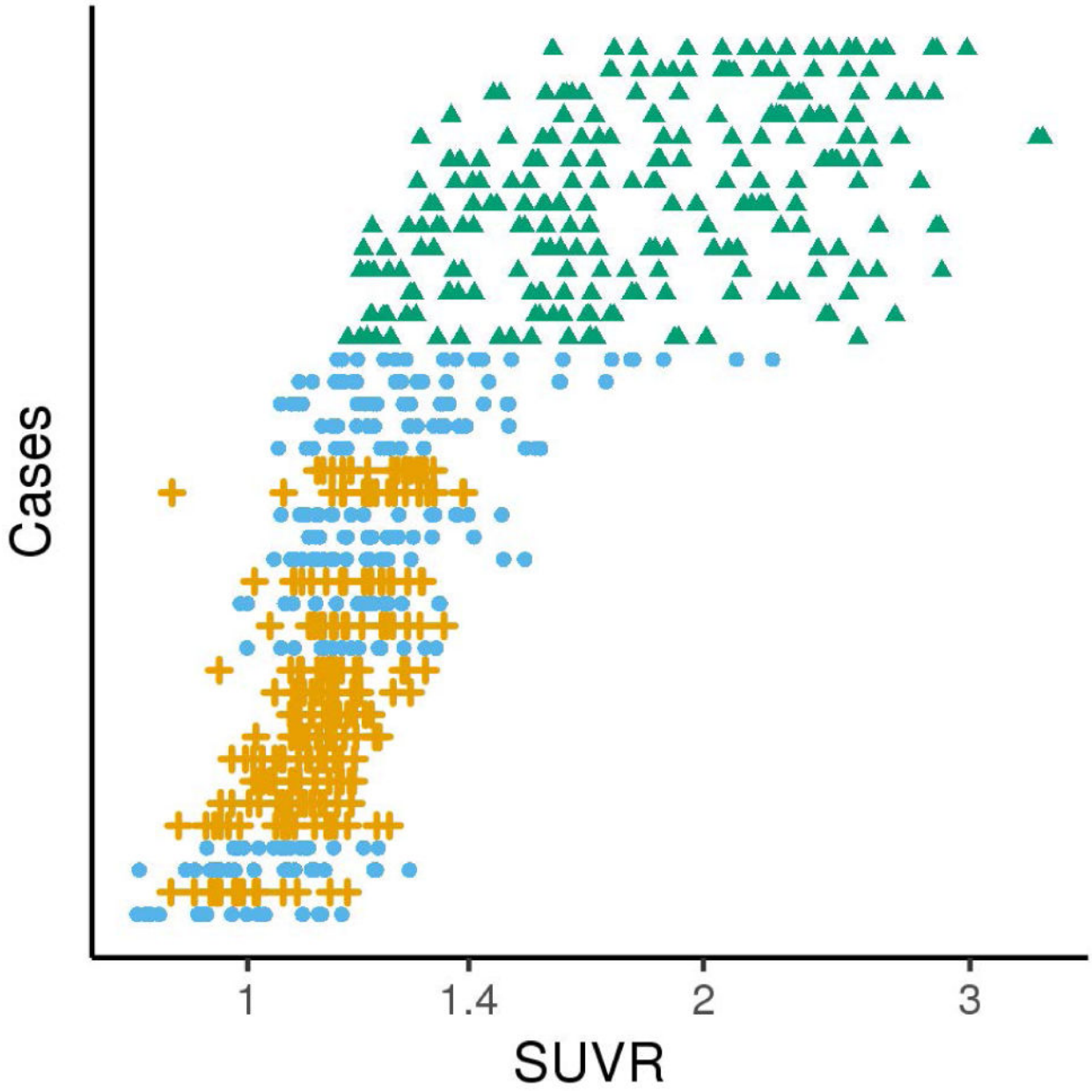

Figure 4.

[^{18}F]AV-1451 SUVRs for all nine ROIs (left and right), for each hemisphere, on a log scale. The 40 PPA cases are displayed by descending mean SUVR across all 18 ROIs from top to bottom. As can be seen, the lvPPA patients (green triangles) had the highest [^{18}F]AV-1451 SUVRs while SUVRs across all ROIs overlapped between agPPA (orange crosses) and svPPA (blue circles) patients.

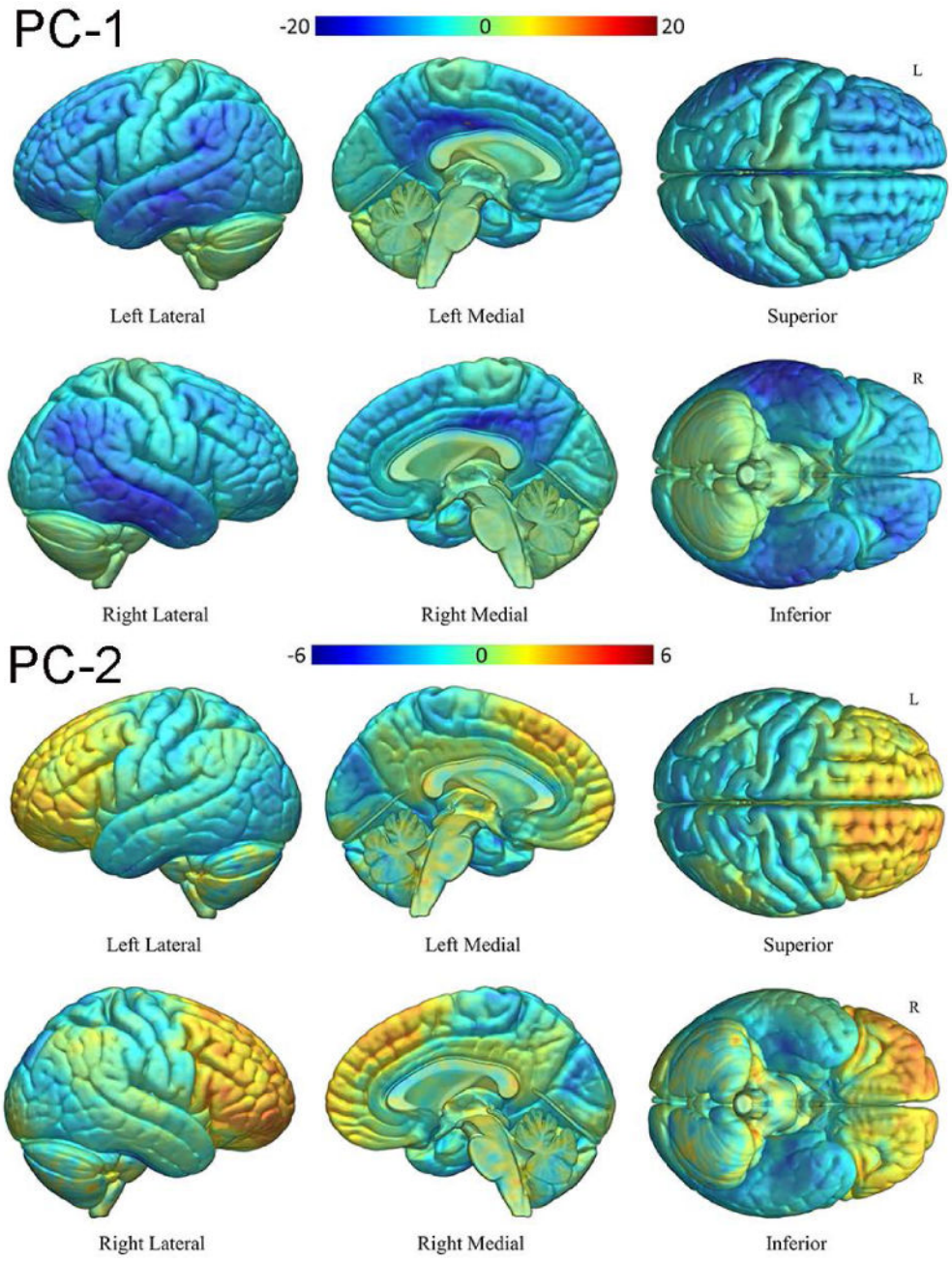

Figure 5.

T-maps for the correlation between PC-1 and PC-2 loading and voxel-wise [^{18}F]AV-1451 uptake, with cool colors showing regions of negative correlation (i.e. voxels where a lower PC load is associated with higher [^{18}F]AV-1451 uptake) and warm colors showing regions of positive correlation.

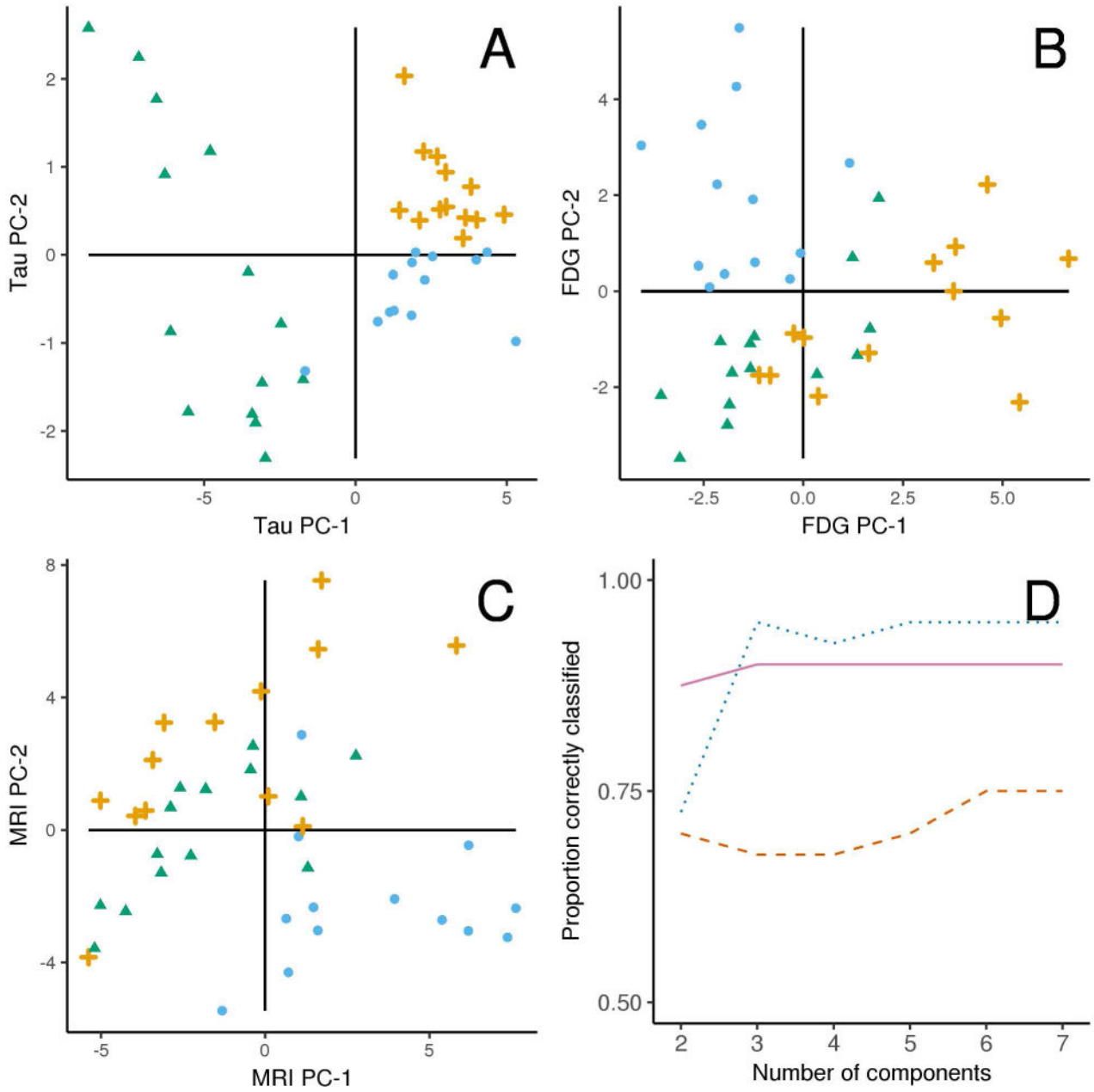

Figure 6.

Plots illustrating the results of the principal component analyses for [^{18}F]AV-1451 uptake (Panel A), FDG-PET metabolism (B) and MRI volumes (C). Each plot shows the three PPA variants according to the first two principal components within a modality, with PC-1 on the X-axis and PC-2 on the Y-axis. The three PPA variants, lvPPA (green triangles), agPPA (orange crosses), and svPPA (blue circles) separate perfectly with [^{18}F]AV-1451 with two principal components, with less than perfect separation in FDG-PET and MRI modalities. Panel D compares penalized multinomial regression models containing increasing numbers of components on the X-axis by their predictive accuracy on the Y-axis in these 40 cases. With 2 components, tau-PET (solid violet line) classification is the highest while with 3 or

more components FDG-PET (dotted blue line) shows the best discrimination. MRI (dashed red line) had the lowest classification accuracy in all instances.

Table 1

Demographic and clinical variables stratified by diagnosis on the 40 PPA subjects

Variable*	agPPA (N=13)	lvPPA (N=14)	svPPA (N=13)	Total (N=40)
Male sex	6 (46%)	2 (14%)	7 (54%)	15 (38%)
Age at tau scan, years	65 (58, 72)	68 (59, 73)	67 (63, 71)	67 (60, 72)
Global PiB	1.29 (1.20, 1.32)	2.49 (2.19, 2.87)	1.31 (1.25, 1.50)	1.43 (1.27, 2.26)
Right handedness	12 (92%)	13 (93%)	13 (100%)	38 (95%)
Disease duration, years	2 (2, 3)	2 (2, 3)	4 (2, 5)	3 (2, 4)
Education	14 (12, 16)	16 (14, 18)	16 (14, 16)	16 (14, 16)
Cambridge Behavioral Inventory/180	34 (18, 48)	16 (13, 26)	46 (34, 64)	33 (14, 58)
Praxis from WAB/60	56 (52, 58)	58 (56, 60)	60 (59, 60)	59 (57, 60)
MDS-UPDRS III/132	4 (2, 9)	2 (2, 4)	0 (0, 3)	2 (0, 5)
Montreal Cognitive Assessment/30	21 (18, 23)	20 (18, 22)	20 (18, 24)	20 (18, 23)
The Neuropsychiatry Inventory/36	5 (3, 10)	2 (0, 3)	7 (4, 11)	4 (2, 8)
Faces recognition/10	10 (10, 10)	10 (9, 10)	4 (1, 7)	10 (7, 10)
Animal fluency	7 (4, 12)	10 (8, 13)	7 (4, 8)	8 (5, 11)
Letter fluency (FAS) sum	8 (5, 10)	29 (24, 32)	25 (17, 30)	25 (17, 32)
SYDBAT naming/30	21 (18, 25)	18 (16, 22)	5 (3, 9)	15 (8, 21)
SYDBAT semantic task/30	24 (20, 28)	27 (24, 27)	14 (10, 19)	22 (15, 27)
Repetition Boston Diagnostic/10	7 (5, 8)	8 (6, 8)	9 (8, 10)	8 (7, 9)
Pyramids & Palm Tree (word-word)/52	46 (42, 49)	49 (48, 51)	39 (38, 42)	45 (40, 49)
Trail making test A, second	55 (47, 90)	51 (44, 70)	48 (29, 58)	50 (39, 69)
Trail making test B, seconds	170 (124, 197)	150 (141, 164)	111 (80, 136)	138 (101, 166)
Rey-O raw score/36	28 (22, 28)	22 (18, 28)	31 (30, 33)	28 (21, 31)
VOSP letters/20	20 (19, 20)	19 (18, 20)	20 (19, 20)	20 (19, 20)
VOSP cubes/10	8 (6, 9)	9 (7, 10)	10 (9, 10)	9 (8, 10)
Digit span	8 (8, 12)	11 (9, 14)	16 (14, 19)	13 (10, 15)
Spatial span	9 (7, 12)	13 (11, 14)	13 (11, 15)	13 (11, 14)
Camden Recognition Memory (faces)/25	22 (18, 24)	24 (22, 24)	20 (18, 23)	22 (18, 24)
Northwestern Anagram Test/10	5 (3, 5)	7 (6, 8)	10 (9, 10)	8 (5, 10)

*Where applicable, the maximum score is shown after a slash

Summaries are reported as n (percent) or median (25th percentile, 75th percentile).

VOSP = Visual Object and Space Perceptual Battery; WAB = Western Aphasia Battery; SYDBAT = Sydney Language Battery; MDS-UPDRS III = Movement Disorders Society - Sponsored Revision of the Unified Parkinson's Disease Rating Scale (Motor Examination)

Table 2

Loadings of the first two principal components on log (tau-PET SUVR) values

Region	PC1 loadings	PC2 loadings
Broca's Area L	−0.24	0.21
Broca's Area R	−0.22	0.38
Entorhinal Cortex L	−0.23	−0.27
Entorhinal Cortex R	−0.22	−0.18
Fusiform L	−0.23	−0.32
Fusiform R	−0.23	−0.29
Inferior Parietal L	−0.24	−0.10
Inferior Parietal R	−0.24	−0.07
Lateral Prefrontal L	−0.25	0.20
Lateral Prefrontal R	−0.24	0.32
Lateral Temporal L	−0.25	−0.21
Lateral Temporal R	−0.25	−0.14
Medial Frontal L	−0.24	0.19
Medial Frontal R	−0.23	0.25
Orbitofrontal L	−0.24	0.18
Orbitofrontal R	−0.22	0.28
Temporal Pole L	−0.23	−0.25
Temporal Pole R	−0.23	−0.18